

# Probing the structural requirements of A-type Aurora kinase inhibitors using 3D-QSAR and molecular docking analysis

Hui-xiao Zhang · Yan Li · Xia Wang · Yong-hua Wang

Received: 6 December 2010 / Accepted: 14 March 2011 / Published online: 28 April 2011  
© Springer-Verlag 2011

**Abstract** Aurora-A, the most widely studied isoform of Aurora kinase overexpressed aberrantly in a wide variety of tumors, has been implicated in early mitotic entry, degradation of natural tumor suppressor p53 and centrosome maturation and separation; hence, potent inhibitors of Aurora-A may be therapeutically useful drugs in the treatment of various forms of cancer. Here, we report an *in silico* study on a group of 220 reported Aurora-A inhibitors with six different substructures. Three-dimensional quantitative structure–activity relationship (3D-QSAR) studies were carried out using comparative molecular field analysis (CoMFA) and comparative molecular similarity indices analysis (CoMSIA) techniques on this series of molecules. The resultant optimum 3D-QSAR models exhibited an  $r_{cv}^2$  value of 0.404–0.582 and their predictive ability was validated using an independent test set, ending in  $r_{pred}^2$  0.512–0.985. In addition, docking studies were employed to explore these protein–inhibitor interactions at the molecular level. The results of 3D-QSAR

and docking analyses validated each other, and the key structural requirements affecting Aurora-A inhibitory activities, and the influential amino acids involved were identified. To the best of our knowledge, this is the first report on 3D-QSAR modeling of Aurora-A inhibitors, and the results can be used to accurately predict the binding affinity of related analogues and also facilitate the rational design of novel inhibitors with more potent biological activities.

**Keywords** Aurora-A · Inhibitor · 3D-QSAR · CoMFA · CoMSIA · Molecular docking

## Introduction

Mammalian Aurora kinases comprise a family of three highly homologous serine/threonine kinases, namely Aurora-A, -B, and -C, which are involved in regulating multiple steps of mitosis, including centrosome duplication, formation of a bipolar mitotic spindle, alignment of chromosomes on the mitotic spindle, establishment and maintenance of the spindle checkpoint, and cytokinesis [1–5]. Since their discovery in 1995 [6], and the first observation of their expression in human cancer tissue in 1998 [7], these kinases have been the subject of intense research in both the academic and industrial oncology communities as novel attractive targets for anticancer therapy [8]. The biology of the three isoforms of Aurora kinase (Aurora-A, -B, and -C) has been reviewed extensively [2, 3]. It is found that, although they are very closely related in kinase domain sequence—Aurora B and C are 75% and 72% identical to Aurora A—certain discrepancies still exist in amino acid length and sequence at the N-terminal domain, and in the cellular localization, regulation, and substrate specificity of these kinases [5, 9].

**Electronic supplementary material** The online version of this article (doi:10.1007/s00894-011-1042-3) contains supplementary material, which is available to authorized users.

H.-x. Zhang · X. Wang · Y.-h. Wang (✉)  
Center of Bioinformatics, Northwest A&F University,  
Yangling, Shaanxi 712100, China  
e-mail: yh\_wang@nwsuaf.edu.cn

Y. Li  
School of Chemical Engineering,  
Dalian University of Technology,  
Dalian, Liaoning 116012, China

Y. Li  
Lab of Pharmaceutical Resource Discovery,  
Dalian Institute of Chemical Physics,  
Graduate School of the Chinese Academy of Sciences,  
Dalian, Liaoning 116023, China

Aurora A localizes to the centrosome and the mitotic spindle from prophase to telophase, and plays a critical role in regulating many early mitotic events, including entry into mitosis [7, 10, 11]. Depletion of Aurora-A results in delayed entrance into mitosis and formation of numerous monopolar spindles due to defects in centrosome maturation and separation and in the organization of the microtubules that form the spindle [8]. Aurora-A can phosphorylate Cdc25b, a direct regulator of the cyclin B1-Cdk1 complex whose activation is an essential requirement for mitotic entry [12]. In addition, phosphorylation of the kinesin motor protein HsEg5 (KSP)—a crucial driver of centrosome separation—by Aurora-A is associated with the later process of centrosome separation as the bipolar spindle forms [13]. Aurora-A is critical to the regulation of the EXTAK multiprotein complex comprised of the proteins Eg5, XMAP2154, TPX-2, Aurora-A, and HURP, which together act to bundle, crosslink, and stabilize the growing microtubule network [8]. Disruption of any component in the complex would perturb spindle formation and lead to mono- and multi-polar spindles [12]. Moreover, Aurora A can promote mdm2-mediated degradation of the natural tumor suppressor p53 and inhibition of its transcriptional activity [14, 15].

The Aurora-A gene lies within a region of chromosome 20q13 that is frequently amplified in many human cancers [7], and is also associated with the chromosomal instability phenotype in colorectal cancers [16]. Overexpression of Aurora-A has been reported to be transforming in some cell types [7, 10], and appears to associate with a wide variety of tumors, including those from colon [7], breast [10], ovary [17], pancreas [18], head, and neck [19]. In addition, transgenic mice overexpressing Aurora-A in the mammary gland develop mammary tumors at a high incidence rate [20]. These results provide compelling evidence that Aurora-A acts as an oncogene and plays a key role in cell cycle progression and carcinogenesis—an area that is emerging as a promising molecular targeted cancer treatment option.

A number of small molecule inhibitors of Aurora kinases have been developed, and more than ten such inhibitors have entered early clinical assessment [8]. ZM447439, a quinazoline derivative and the first Aurora kinase inhibitor to be developed in 2003, inhibits both Aurora-A and -B (IC<sub>50</sub> values of 110 and 130 nM, respectively) [21]. VX-680/MK-0457, which is a 4,6-diaminopyrimidine that inhibits all three Aurora kinases (A, B, and C) with *K<sub>i</sub>* values of 0.6, 1.8, and 4.6 nM, respectively, and was first demonstrated in 2004 to show potent antitumor activity in vivo [22]. Hesperadin is an indolinone inhibitor of Aurora-B (IC<sub>50</sub> of 250 nM) with significant cross-reactivity against six other kinases (no data on Aurora-A or -C are reported) [23]. Examples of Aurora selective inhibitors include AZD1152 (the first Aurora-B selective inhibitor to enter clinical trials) [24], MLN8054 (the first reported Aurora-A

selective inhibitor) [25], and the most recently developed inhibitor, MK-5108 (Aurora-A selective) [26]. These Aurora inhibitors, which have diverse structures and biological activities, offer the potential to improve the treatment of cancer by helping to develop new drugs as well as by defining optimal therapeutic strategies.

In silico modeling has been demonstrated as one of the most widely used and effective tools in reducing costs and speeding up the drug discovery process. Nowadays, it has become an urgent task to design more potent Aurora inhibitors in order to present new strategies to identify therapeutics for cancer treatment. In order to understand the function–structure relationships of Aurora inhibitors, simple explorations based on the derivatives of some effective inhibitors have been carried out [8, 9, 27, 28]. Furthermore, crystallography studies have shown that the Aurora kinases can adopt a number of different conformations that represent distinct drug targets with alternative opportunities to derive potency and selectivity [8]. For instance, the crystal structure of VX-680 with Aurora-A kinase showed that the compound is bound to an “inactive-closed” conformation of the enzyme, and that the cyclopropyl group of the amide occupies a small hydrophobic pocket capped by a phenylalanine residue (Phe275). However, the crystal structures of activated “open” Aurora-A show that this pocket is not available in this conformation [8]. The crystal structure of Aurora-A and TPX2 illustrated that TPX2 makes two contacts with the Aurora-A kinase domain. The interactions between TPX2 and Aurora-A help mold the activation loop into a conformation that is ready for substrate binding, and also provide a lever arm-like mechanism that causes the rotation of phosphorylated T288 away from the solvent-exposed position found in free Aurora-A, thus protecting it from dephosphorylation by PP1 [29]. Recently, a structural study revealed the potential importance of Thr217 by revealing a hydrogen-bonding interaction with pyrazole compounds that exhibit specificity for Aurora A over Aurora B [28]. Despite the many co-complex structures that have been solved, in most cases a clear explanation for the observed inhibitory activity against Aurora kinases is still unclear. To date, a comprehensive review of the structural requirements of Aurora-A inhibitors based on quantitative structure–activity relationship (QSAR) has not been reported, highlighting the urgency of undertaking such studies to fill the blank in this field. Thus, in this work, two widely used QSAR methods, i.e., comparative molecular field analysis (CoMFA) and comparative molecular similarity indices analysis (CoMSIA) [30, 31], were exploited to derive 3D-QSAR models for six different chemical series of Aurora-A inhibitors. These techniques were applied successfully in the past to various therapeutic areas in our laboratory [32–36]. In addition to 3D-QSAR analyses, docking

simulations were also performed to explore the molecular interactions between ligands and their receptors at the active site. To the best of our knowledge, this is the first attempt toward the establishment of 3D-QSAR for A-type Aurora inhibitors, which may help in designing and forecasting the Aurora-A inhibitory activity of novel molecules.

## Materials and methods

### Dataset

In order to build as large a dataset as possible, while still maintaining consistency of structure and bioactivity in generating QSAR models, a total of 220 molecules reported as Aurora-A inhibitors were collected from recently published data [8, 9, 27, 28, 37–41]. These chemicals have diverse structures, and the main skeletons of these molecules can be divided into six main groups (Table 1): Groups GI–GVI, comprise 37, 36, 25, 54, 24, and 44 molecules, respectively. The *in vitro* inhibitory activity,  $K_i$  or  $IC_{50}$  ( $\mu\text{M}$ ) against Aurora-A was converted to  $pK_i$  or  $pIC_{50}$  in developing 3D-QSAR models. For each group, the molecules of the test set represent nearly 25% of the whole dataset. The strategy for selection of training and test sets was to ensure that test compounds represented a similar structural diversity and range of biological activities as the training set. To illustrate this, a principal component analysis (PCA) was performed on the dataset as follows: (1) more than 600 structural descriptors, including the topological, constitutional, walk and path counts, atom-centered fragments and connectivity indices for each molecule, were calculated for all the compounds using Dragon software ([http://www.taletе.mi.it/help/dragon\\_help/](http://www.taletе.mi.it/help/dragon_help/)); (2) PCA was then performed within the calculated structure descriptor space for the whole dataset, giving three significant principal components (PCs) that explain more than 70% of the variation in the data [42]. The structures and inhibitory activity data of the training and test set molecules are described in Tables S1, S2, S3, S4, S5 and S6, and details of distribution of the compounds over the three PCs for each class are depicted in Figs. S1, S2, S3, S4, S5 and S6 (Supporting Information).

### Molecular modeling

The 3D-QSAR and molecular docking computations were carried out using Sybyl 6.9 (<http://tripos.com/>) on a Redhat Linux platform. The 3D structures of the training and test set compounds were built using the Sketch Molecule function in Sybyl. Optimization of the 3D structures was carried out using TRIPOS force field with the Gasteiger Hückel charges, and repeated minimization was performed

using Powell conjugate gradient method until a root-mean-square (rms) deviation of  $0.001 \text{ kcal mol}^{-1}$  was achieved. Compound alignment was performed separately for each dataset with each respective common structure (Table 1, shown in bold). In each dataset, the most active compound was chosen as the template molecule and all compounds were aligned to a common substructure using the “align database” command in Sybyl software. The corresponding alignment results of the six groups are shown in Figs. S7, S8, S9, S10, S11 and S12 (Supporting Information).

### CoMFA and CoMSIA analyses

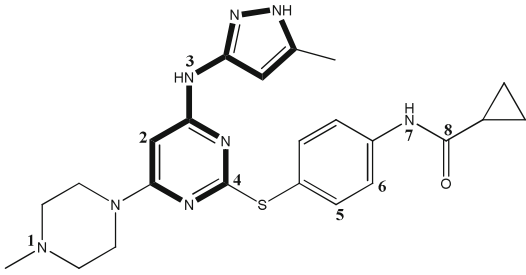
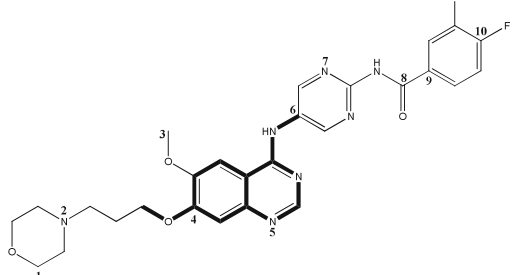
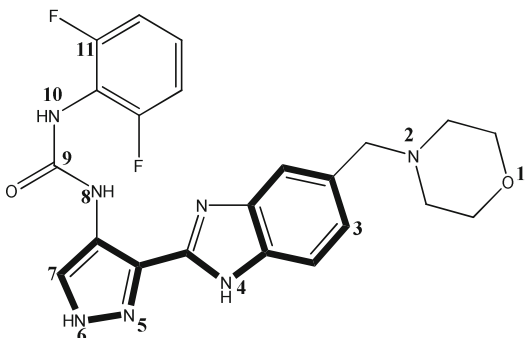
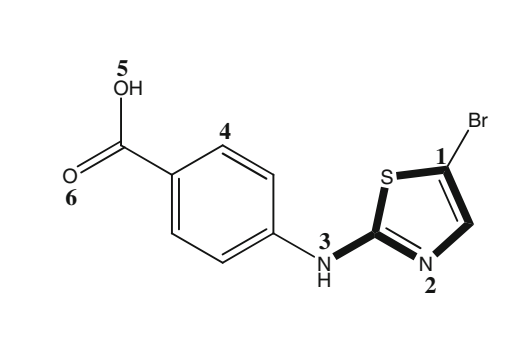
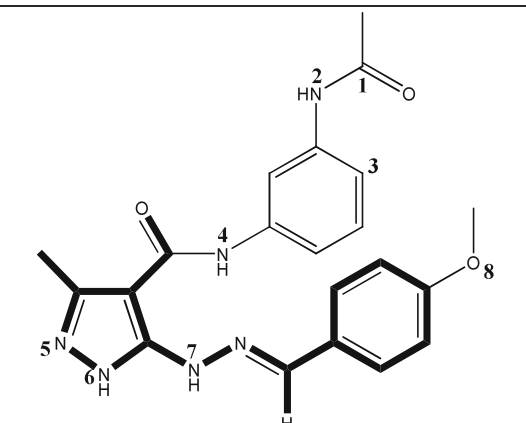
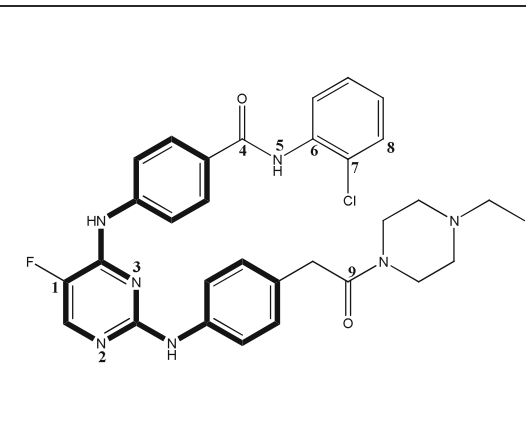
In order to derive the CoMFA and CoMSIA descriptor fields, a 3D cubic lattice with grid spacing of  $2 \text{ \AA}$  in  $x$ ,  $y$  and  $z$  coordinates, was created to encompass the aligned molecules. CoMFA descriptors were calculated using an  $sp^3$  carbon probe atom with a van der Waals radius of  $1.52 \text{ \AA}$  and a charge of  $+1.0$  to generate steric (Lennard-Jones 6–12 potential) field energies and electrostatic (Coulombic potential) fields with a distance-dependent dielectric at each lattice point. The steric and electrostatic cutoff values were set to  $35 \text{ kcal mol}^{-1}$  for group II and  $30 \text{ kcal mol}^{-1}$  (default value) for the remaining groups, which are optimal parameters for the respective models. In CoMSIA analyses, the steric, electrostatic, hydrophobic, and hydrogen-bond donor and acceptor descriptors were calculated using the probe atom  $C_{sp^3}^+$  with a radius of  $1 \text{ \AA}$  and a  $+1.0$  charge placed at the lattice points of the same region of the grid as used for CoMFA calculations.

Partial least-square (PLS) regression analyses was used to evaluate the predictive values of models using the leave-one-out (LOO) cross validation method. The number of components leading to the highest cross-validated  $r^2$  and lowest standard error of prediction was set as the optimum number of components in the PLS analyses;  $F$  value and standard error of estimates (SEE) were then calculated. The models were also evaluated for their ability to predict the activity of compounds in the test set. A detailed description of this method can be found in many previous works [32, 35, 36].

### Molecular docking

Molecular docking analysis was carried out using the Surflex module of the Sybyl package to explore the interaction mechanism and to illustrate the accurate binding model for the active site of Aurora-A with its ligands [43]. Up to now, 38 various Aurora-A crystal structures complexed with different inhibitors have been reported in the RCSB Protein Data Bank (<http://www.pdb.org>). To ensure reasonable docking models, the selection of Aurora-A crystal structures was made according to the following criteria:

**Table 1** Main skeletons (shown in bold) and template molecular structures in each group with corresponding inhibitory activities ( $pK_i$  or  $pIC_{50}$ ) for Aurora-A kinase

Group I		Group II	
			
Compound	$pK_i$ ( $\mu\text{M}$ )	Compound	$pIC_{50}$ ( $\mu\text{M}$ )
37	3.222	68	3.824
Group III		Group IV	
			
Compound	$pIC_{50}$ ( $\mu\text{M}$ )	Compound	$pIC_{50}$ ( $\mu\text{M}$ )
81	2.824	119	1.102
Group V		Group VI	
			
Compound	$pIC_{50}$ ( $\mu\text{M}$ )	Compound	$pIC_{50}$ ( $\mu\text{M}$ )
176	1.481	220	2.469

- (1) The ligand in the crystal structure to be applied should share a common structure with certain group compounds; also, the most active compound in the corresponding dataset should have a reasonable docking score (total score of 5.96 on average) in obtaining the models. Therefore, the following PDB files were used: 3E5A for G-I [44], 2C6E for G-II [40], 2W1E for G-III [38], 3FDN for G-V [28], and 2NP8 for G-VI [45].
- (2) For the remaining group, G-IV, no common structure was observed with any of the ligands in the X-ray complexes. In this case, the file 1MUO.pdb [46] was selected as the co-crystallized ligand shares several highly topological similarities, such as molecular size, shape, distribution of H-bond donors/acceptors with the most active compound **119** in G-IV.

In Surflex-docking, protomol construction was based on protein residues proximal to the native ligand and on parameter settings to produce a small and buried docking target. Two parameters, i.e., `protomol_bloat` and `protomol_threshold`, which determine how far from a potential ligand the site should extend, and how deep into the protein the atomic probes used to define the protomol can penetrate, were adjusted to produce reasonable docking results (for detailed values, see section on [Docking analysis and comparison with 3D contour maps](#) below). For receptor preparation, all ligands were first removed and the polar hydrogen atoms were added. Water molecules in 3E5A, 2C6E, 2W1E, 3FDN and 2NP8 crystal structures were not removed for the reason that co-crystallized water molecules were found in the active site and could be involved in ligand–protein interactions by forming mediating H-bonds between the ligand and the protein. No water molecules were considered for docking with G-IV, since this protein receptor 1MUO.pdb has no co-crystallized water molecules in the active site. Automatic Mode was adopted to generate the protomol, and other parameters used the default values of this software.

## Results and discussion

All combinations of CoMFA and CoMSIA models for the 220 compounds were calculated and analyzed; only the optimal 3D-QSAR models for each class are listed in Table 2. The best models were selected primarily on the basis of better cross-validated  $r^2$  and predictive  $r^2$  values and the chosen models were then exploited to generate 3D contour maps. In addition, a parameter,  $r_m^2$ , was included to validate the external predictability of QSAR models, and a value of  $r_m^2 > 0.5$  could be taken as an indicator of good external predictability [47]. The plot of actual versus

predicted activities for the training and test set molecules for each class is depicted in Fig. 1, where the data points are rather uniformly distributed around the regression line, indicating that the obtained models are reasonable.

In 3D-QSAR analyses, one of the major obstacles lies with the ‘congeners’, which misfit the final equation and are termed as outliers. In our study, several factors may account for the outliers: (1) unique structural differences such as compounds **20** and **29**, which have a  $-t\text{Bu}$  substituent in the GI series; (2) different binding conformations like compounds **145** and **166** that have very low binding affinity in docking analysis (2.72 and 3.32, respectively); and (3) a higher residual between the observed and predicted biological activity, as in the case of compounds **71** and **199**, which have residuals more than 1 log unit. All these compounds were deleted from the data set, and the 3D-QSAR models were derived from the remaining compounds; the resulting models served as the basis for further assessment and discussion.

## Graphical interpretation of the 3D-QSAR models

One of the attractive features of 3D-QSAR modeling is that the results can be visualized as 3D coefficient contour plots. To aid the visualization, the most potent molecule in each group of compounds is displayed and discussed as the reference compound. In order to select appropriate contour levels for each feature, the resulting histograms of actual field values were analyzed, and a contour level was chosen interactively as that producing the best interpretable contour map.

### Group-I

In Fig. 2a, the yellow contours near position 2 indicate that bulky substituents at this position are not favorable for inhibitory activity. This is in accordance with the findings of Pollard et al. [8], showing that improvements in bioactivity were obtained upon replacement of the quinazoline with 6-heterocyclic substituted pyrimidines (compounds **21** and **32–34**). A large, sterically unfavorable, yellow polyhedron is seen near positions 4 and 5. In the CoMSIA electrostatic field, the blue contour observed near positions 5 and 6 indicates that a negatively charged group at these positions would have a detrimental effect on biological activity. The red contour near position 8 suggests the favorability of electronegative groups for inhibitory activity (compounds **16**, **17** and **37**). Figure 2c shows the contour map of the hydrophobic field with compound **37** overlaid. In the CoMSIA hydrophobic field, a large white contour seen in the vicinity of positions 7 and 8 indicates that a hydrophilic substituent at these positions is favored for inhibitory activity. There is also a small yellow region

**Table 2** Summary of statistical results of the optimal three-dimensional quantitative structure–activity relationship (3D-QSAR) models for each of the six groups GI–GVI.  $r_{cv}^2$  Cross-validated correlation coefficient using the leave-one-out (LOO) methods,  $N_C$  optimal number of components,  $SEP$  standard error of prediction,  $r_{ncv}^2$  non-cross-validated correlation coefficient,  $SEE$  standard error of estimate,  $r_{pred}^2$  predicted correlation coefficient for the test set of compounds,  $S$  steric,  $E$  electrostatic,  $H$  hydrophobic,  $D$  H-bond donor,  $A$  H-bond acceptor

	G-I	G-II	G-III	G-IV	G-V	G-VI
	CoMSIA	CoMFA	CoMSIA	CoMSIA	CoMSIA	CoMSIA
$r_{cv}^2$	0.501	0.404	0.582	0.432	0.549	0.454
$N_C$	7	6	6	6	4	6
$SEP$	0.135	0.333	0.241	0.288	0.048	0.280
$r_{ncv}^2$	0.982	0.973	0.982	0.809	0.986	0.964
$SEE$	0.089	0.216	0.168	0.240	0.083	0.151
$F$ value	147.609	119.974	110.034	21.838	205.669	110.175
$r_{pred}^2$	0.946	0.809	0.928	0.512	0.985	0.719
$r_m^2$	0.890	0.552	0.838	0.507	0.975	0.662
Contribution (%)						
S	25.6	45.4	43.1	21.3	12.0	13.7
E	28.0	54.6	56.9	25.8	58.6	44.9
H	46.4	-	-	-	-	41.4
D	-	-	-	-	29.4	-
A	-	-	-	52.9	-	-

near the white contour, suggesting that a hydrophobic substituent around this yellow region would also enhance inhibitory activity. In addition, a white contour observed near position 1 signifies that the introduction of hydrophilic group at this position would improve inhibitory effects on the enzyme (compounds **36** and **37**).

### Group-II

The steric contour plot of the best model with the template molecule (compound **68**) is shown in Fig. 3a. The green contour observed near position 6 suggests that bulky substituents may favor activity, yet the yellow contour near

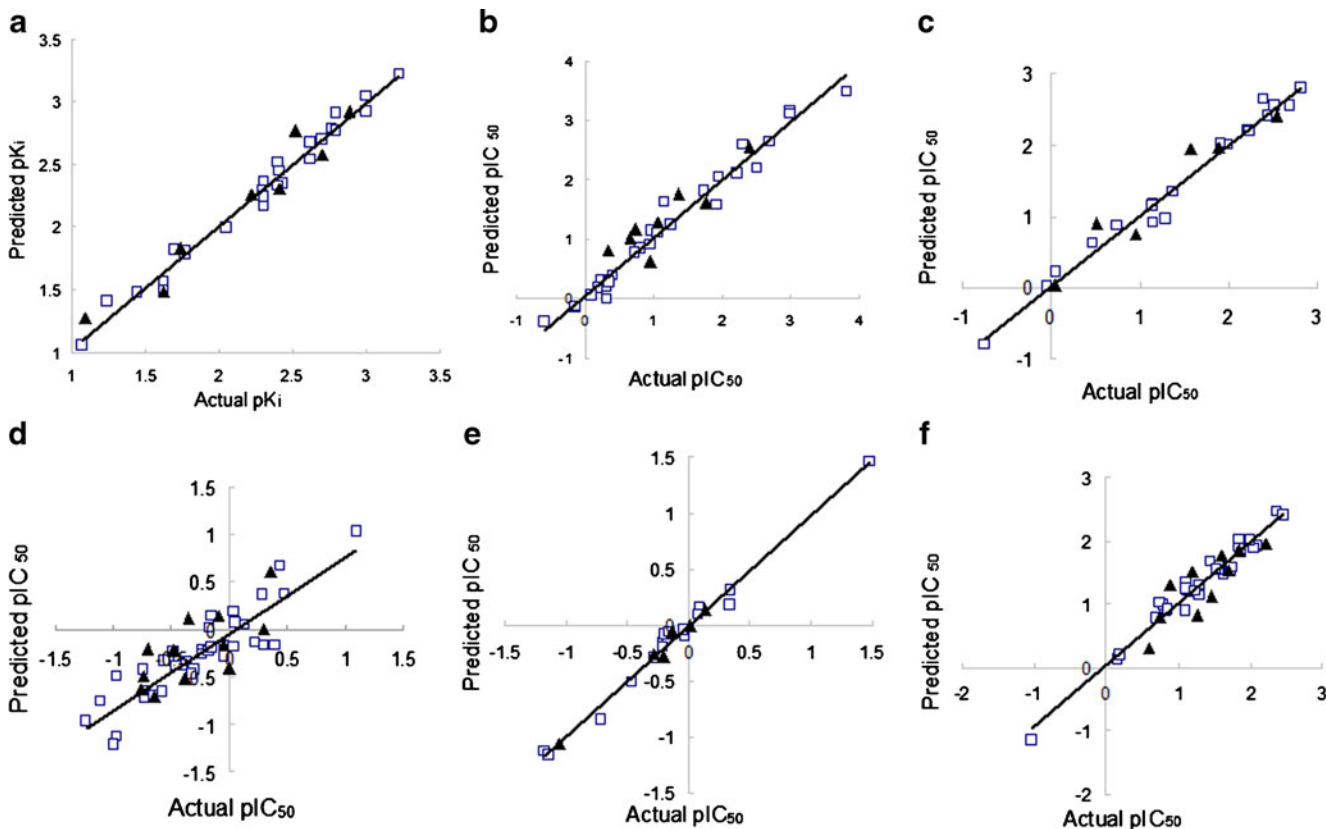


**Fig. 1** Plots of the predicted versus experimental activity data of the optimal three-dimensional quantitative structure–activity relationship (3D-QSAR) model in each group (GI–GVI) for the training and the test set compounds. □ Training set, ▲ test set

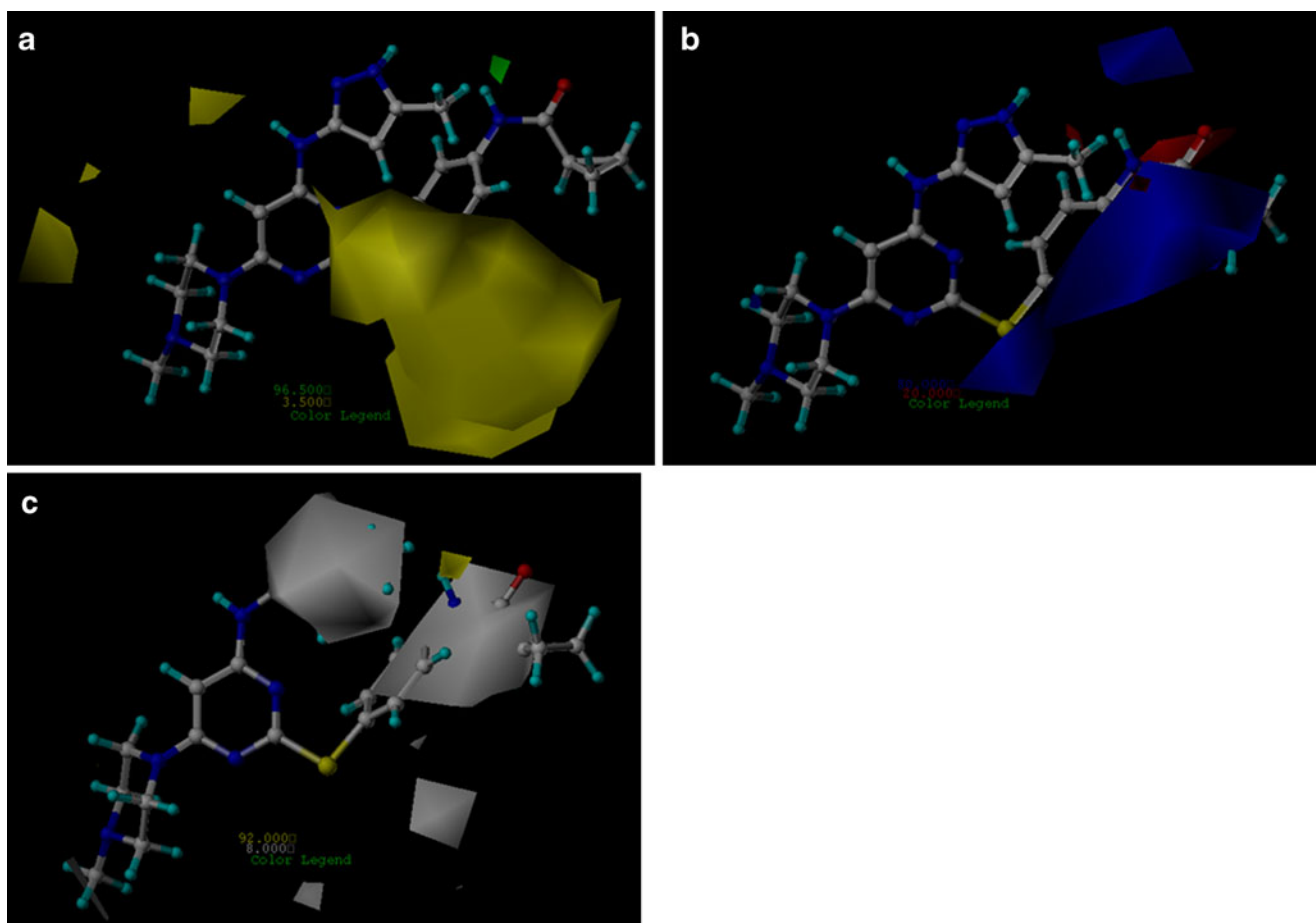


**Fig. 2** Comparative molecular similarity indices analysis (CoMSIA) stdev\*coeff (a) steric, (b) electrostatic and (c) hydrophobic contour maps for Group I. Color code: a green and yellow contours favorable and unfavorable bulky groups, respectively; b blue and red contours

favorable and unfavorable electropositive groups, respectively; c yellow and white contours favorable and unfavorable hydrophobic groups, respectively. Compound 37 in ball and stick is displayed as a reference

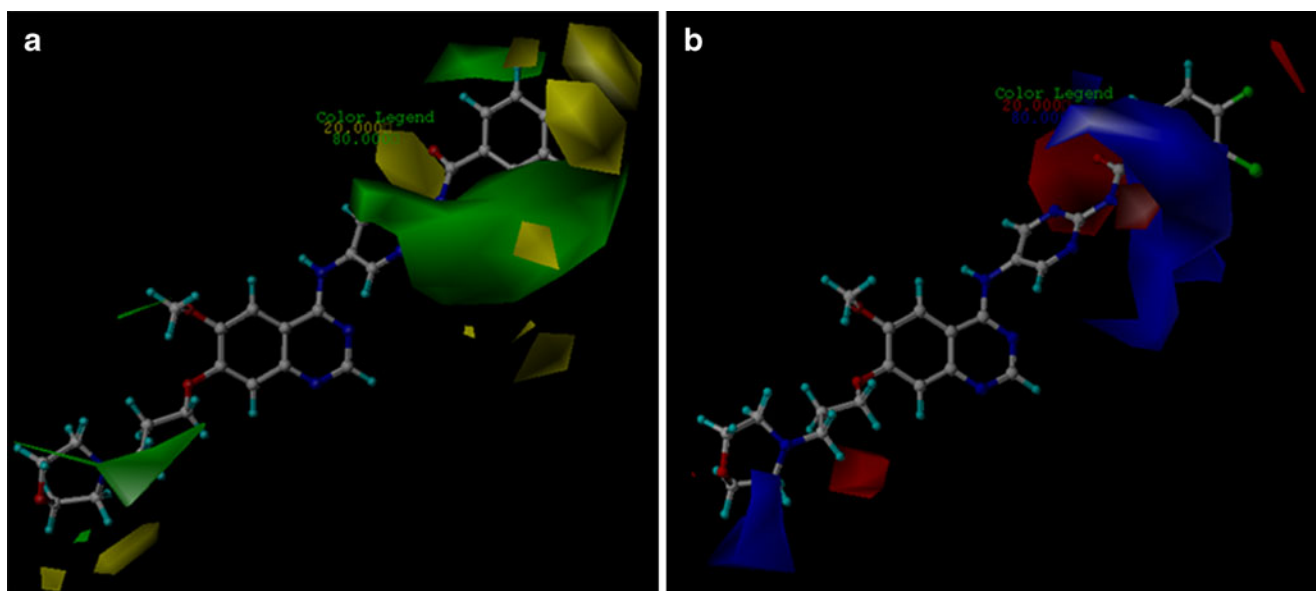


**Fig. 3** Comparative molecular field analysis (CoMFA) stdev\*coeff (a) steric and (b) electrostatic contour maps for Group II. Color codes of a and b as in Fig. 2. The compound 68 in ball and stick is displayed as a reference

position 10 indicates that a bulky substituent would decrease biological activity. A small green contour near position 3 indicates that a sterically bulky group is favored in this region (compounds **45**, **47** and **48**). The electrostatic contour map with the reference compound **68** is described in Fig. 3b. The red contour near position 10 indicates the significance of a negatively charged group for biological activity. The positively charged blue contour near position 1 suggests that a compound activity might be decreased by an electronegative group at this position (compounds **46** and **49**).

#### Group-III

The CoMSIA model of steric contribution is shown in Fig. 4a, with compound **81** overlaid on the map. A large yellow contour near position 7 indicates that compounds like **97** with bulky substituents (–COOEt) entering this yellow region will be less active than those unsubstituted or with small substituents like compounds **94** and **98** (–CH<sub>2</sub>OH). A small green contour at position 10 suggests the requirement for a bulky substituent in this area to enhance biological activity. The CoMSIA electrostatic map is displayed in Fig. 4b. Clearly, a blue region is observed near position 7, suggesting a high demand for positively charged substituent in this region to improve inhibitor activity. The red contour near position 1 indicates that its occupancy by negatively charged groups would favor inhibitory activity, as revealed by compounds **74** and **78**. Another small red contour near position 11 suggests an electronegative group is preferred in this region (compounds **79** and **80**).

#### Group-IV

For the CoMSIA steric model (Fig. 5a, with compound **119**), a large green contour at position 4 suggests that

occupancy of this sterically favorable region with a bulky substituent would lead to an increase in bioactivity. The green contour located near position 1 indicates that a bulky substituent is preferred at this position (compounds **145** and **146**). Figure 5b showed the CoMSIA electrostatic contour plot with compound **119** overlaid on the map. The blue contour plot near position 4 indicates that an electropositive group is favorable. This is consistent with the experimental results that compound **130** shows higher activity than **129** and **131** since **130** has a more electropositive group (3-Me) than **129** (3-F) and **131** (3-CF<sub>3</sub>) in this region. In the H-bond acceptor contour map (Fig. 5c), the red contour near position 5 indicates that an H-bond donor group is favored as supported by the fact that compound **119** is more active than **118** since **119** has an H-bond donor group (–OH) herein while **118** does not (–OEt). The magenta contour observed near position 4 suggests that the H-bond acceptor enhanced molecular activity.

#### Group-V

The graphical representation of the CoMSIA steric field with reference compound **176** is displayed in Fig. 6a. The green contour near position 1 suggests that a bulky substituent may be necessary to increase the inhibitory potency of the compound. A large yellow contour located at position 3 indicates that bulky substituents have unfavorable steric interactions (compounds **169**, **173** and **175**). In CoMSIA electrostatic field (Fig. 6b with compound **176**), a positive charge favored blue contour is observed near position 4, which is in accordance with the finding of Coumar et al. [28], that replacement of O with NH at this position would enhance compound activity. The graphical representation of CoMSIA H-bond donor field is shown in Fig. 6c. A small cyan contour near position 4 indicates that the H-bond donor group is favorable for activity. This is verified by experiment results that compound **157** exhibits

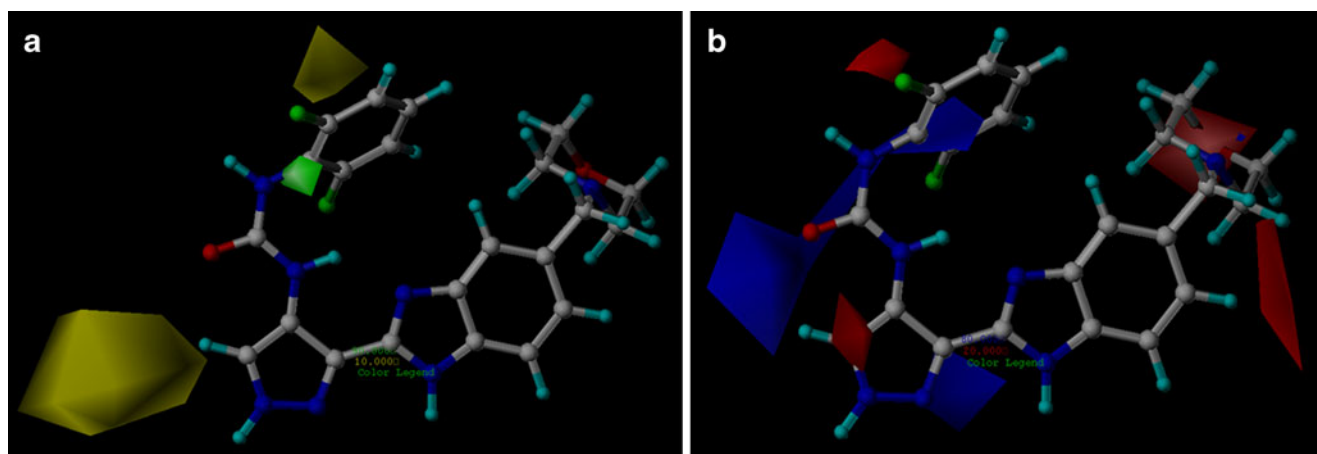


**Fig. 4** CoMSIA stdev\*coeff (a) steric and (b) electrostatic contour maps for Group III. Color code of a and b as in Fig. 2. The compound **81** in ball and stick is displayed as a reference

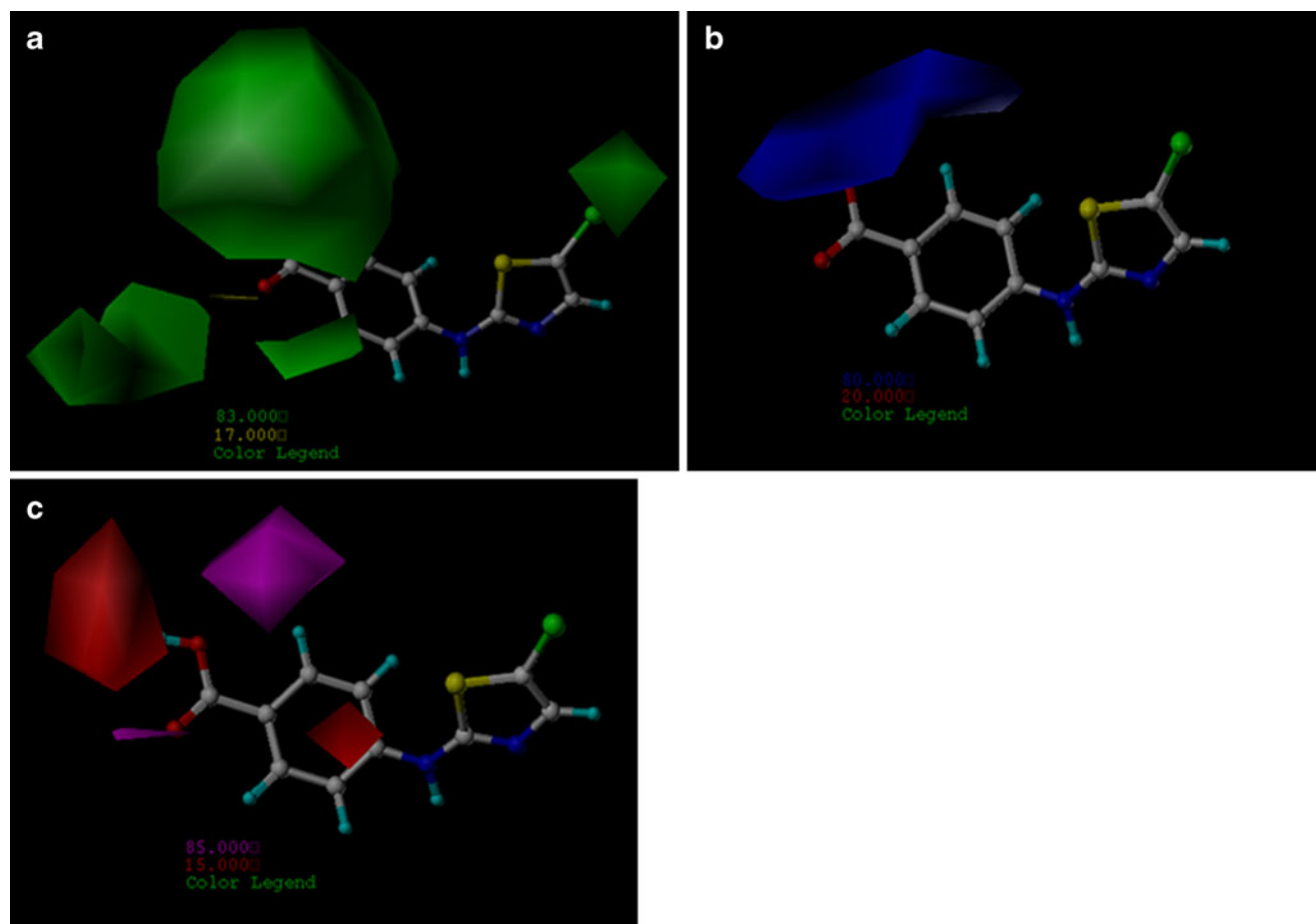


**Fig. 5** CoMSIA stdev\*coeff (a) steric, (b) electrostatic and (c) H-bond acceptor contour maps for Group IV. Color code for a and b as in Fig. 2; c magenta and red contours favorable and unfavorable

H-bond acceptor groups, respectively. The compound **119** in ball and stick is displayed as a reference

higher activity than **156** since **157** has an H-bond donor group ( $-\text{NH}-$ ) at this position while **156** does not ( $-\text{O}-$ ). A purple contour near position 1 suggests there would be a positive effect on biological activity by having an H-bond acceptor replaced in this region.

#### Group-VI

The steric contour map of the CoMSIA model with compound **220** is displayed in Fig. 7a. The yellow contour observed near position 1 indicates that a bulky substituent may decrease biological activity, which agrees partly with the finding by Aliagas-Martin et al. [37] that smaller aliphatic groups are preferred at this position (compounds **188**, **189** and **190**). A large green contour is seen near position 6, suggesting that a bulky substituent is favorable in this region, as confirmed by the fact that compounds **200** and **201**, with substituents *i*-Pr and Ph, respectively, show higher activity than unsubstituted analogue **197**. A small green contour near position 9 signifies that occupation of this area by a bulky group would have a positive effect on activity. The electrostatic contour map of the

CoMSIA model with compound **220** is shown in Fig. 7b. A small red contour near position 1 indicates the requirement for increased electron density in this area, which is in accordance with the findings of Aliagas-Martin et al. [37] that electron-withdrawing substituents, especially halogens, are preferred in this region (compounds **181**, **185**, **187** and **189**). The blue contour map observed near position 5 suggests that electro-negative groups are not favored for inhibitory activity (compounds **211** vs **217** and **218** vs **220**). The hydrophobic contour map of the CoMSIA model with compound **220** is shown in Fig. 7c. The white contour near position 8 indicates that its occupancy by a hydrophilic group would enhance activity. A medium size yellow contour located near position 7 suggests that a hydrophobic group is favorable for inhibitory activity (compounds **202**, **205** and **208**).

#### Docking analysis and comparison with 3D contour maps

All the 220 molecules in six different groups were docked into the active site of Aurora-A protein. Prior to docking the inhibitors with the protein crystal structure, a redocking of the

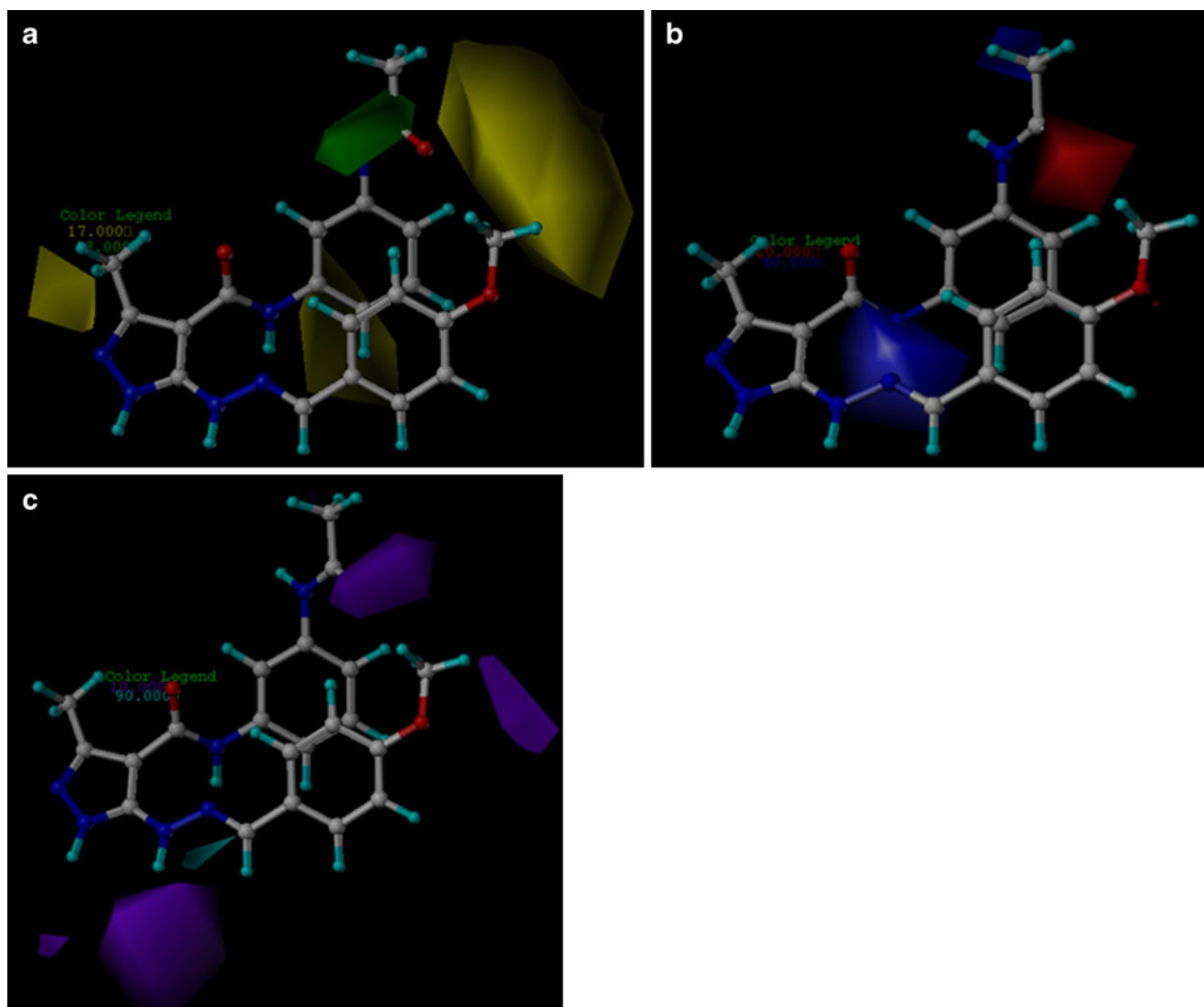


**Fig. 6** CoMSIA stdev\*coeff (a) steric, (b) electrostatic and (c) H-bond donor contour maps for Group V. Color code of **a** and **b** as in Fig. 2; **c** cyan and purple contours favorable and unfavorable

the co-crystallized ligand was performed by removing the ligand from the binding site and redocking it to the binding site of Aurora-A kinase. Our analysis suggests good agreement between the localization of the inhibitor observed upon docking and that from the crystal structure as evidenced by the result that RMSD values in each group (I–VI) were 0.87 Å, 1 Å, 0.34 Å, 0.02 Å, 0.27 Å and 1.5 Å, respectively. The low RMSD values suggest the high docking reliability of Surflex-Dock in reproducing the experimentally observed binding mode for Aurora A kinase inhibitor and the parameter set for Surflex-docking reproduces X-ray structures with reasonable accuracy.

#### Group-I

The protomol bloat and threshold applied the default values (0 and 0.5, respectively) and the binding mode of

H-bond donor groups, respectively. The compound **176** in ball and stick is displayed as a reference

compound **37** is displayed in Fig. 8. The ligand is anchored in the binding site via three H-bonds and one water-mediated contact with the protein. Pyrazole –N– and –NH ring atoms form H-bonds with the backbone at Ala213 (–N⋯HN,  $d_1=2.08$  Å,  $\theta_1=146.8^\circ$ ) and Glu211 (–NH⋯O,  $d_2=2.34$  Å,  $\theta_2=77.1^\circ$ ), respectively. The –NH– nitrogen atom at position 3 forms a H-bond with the carbonyl oxygen atom on the backbone at Ala213 (–NH⋯O,  $d_3=2.24$  Å,  $\theta_3=169.2^\circ$ ). The oxygen atom at position 8 forms a H-bond (2.68 Å,  $144.9^\circ$ ) with water16, which itself forms H-bonds to the backbone –NH of Phe275, side chain –OH of Glu181 and carbonyl oxygen atom of Gln185. Substituents like phenyl directly linked to position 4 would potentially have a steric clash with residue Phe144, as is evident from the presence of a CoMSIA large sterically unfavorable yellow contour. The side chain –NH– of the

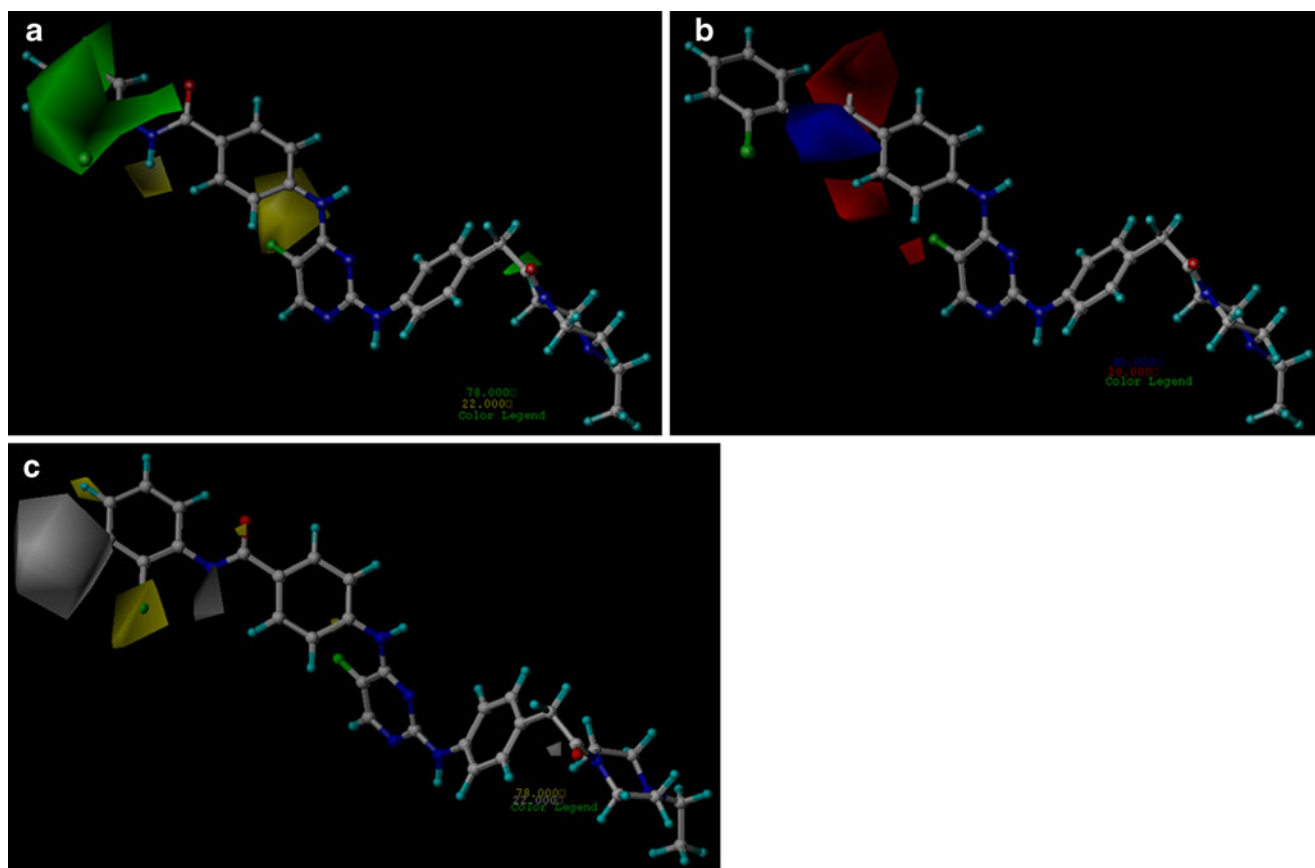


**Fig. 7** CoMSIA stdev\*coeff (a) steric, (b) electrostatic and (c) hydrophobic contour maps for Group VI. Color code for a, b and c as in Fig. 2. The compound **220** in ball and stick is displayed as a reference

Gln185 residue and water molecule (w16, 3E5A.pdb) near position 8 suggests a requirement for an electronegative group like carbonyl, which is in accordance with the CoMSIA red contour observed herein. The presence of

the white contour for the pyrazole ring indicates a hydrophilic favorable region, as confirmed by the docking results that two H-bonds exist in this region between the pyrazole ring and residues Ala213 and Glu211, respectively. According to the docked structure, the small white contour observed near position 1 suggests that the substituent at this position is exposed to the solvent.

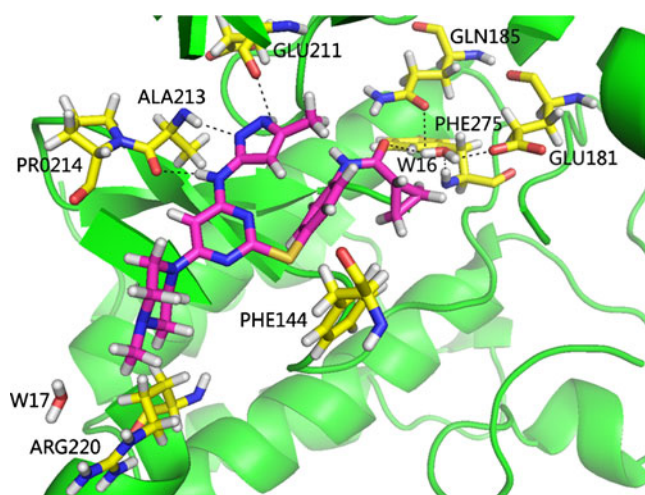
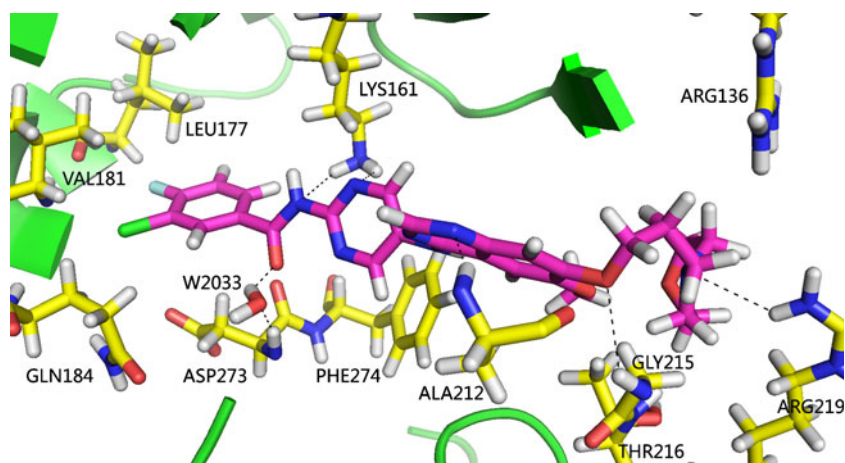


**Fig. 8** Docked conformation derived for compound **37** with the binding site of Aurora-A kinase. H-bonds are shown as dotted black lines. Active site amino acid residues and the inhibitor are represented in stick model. W16 and W17 represent water molecules

#### Group-II

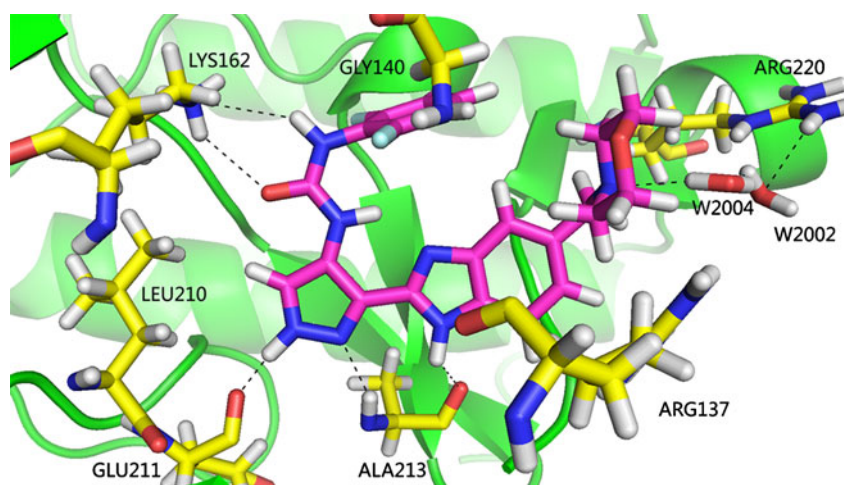
The protomol bloat and threshold values were set to 0 and 0.6, respectively, and compound **68** is shown in Fig. 9. Five H-bonds and one water-mediated interaction exist in the active site of the protein structures. For example, a quinazoline ring nitrogen at position 5 interacts through H-bonding with the backbone of the Ala212 amino acid residue ( $-N\cdots HN$ ,  $d_1=2.25\text{ \AA}$ ,  $\theta_1=160.7^\circ$ ). The nitrogen atom of the morpholine ring at position 2 forms a H-bond with the guanidino group of Arg219 ( $-N\cdots HN$ ,  $d_2=3.09\text{ \AA}$ ,  $\theta_2=127.3^\circ$ ). The pyrimidine ring N atom at position 7 is located within H-bonding distance ( $2.97\text{ \AA}$ ) from the Lys161 side-chain amino function. The water-mediated interaction (i.e., forming H-bonds with proteins through water molecules) is observed between the carbonyl oxygen

**Fig. 9** Docked conformation derived for compound **68** with the binding site of Aurora-A kinase. H-bonds are shown as *dotted black lines*. Active site amino acid residues and the inhibitor are represented as *stick model*. W2033 represents a water molecule



at position 8 and the backbone  $-NH$  of Asp273. The 4-substituent of the quinazoline ring binds to the solvent-exposed pocket, where it interacts with Arg136, Thr216 and Arg219 amino acid residues. Comparing the docked structure and the 3D contour plots reveals that the yellow contour is present in the regions of Leu177 and Val181. Hence, a bulky substitution at position 10 would have an unfavorable steric interaction, which may also explain the lowest activity of compound **73**. Another sterically unfavorable region (yellow contour) is located near the carbonyl oxygen atom at position 8. Our docked model shows that a bulky substituent at this position would have an unfavorable steric clash with the backbone of residue Asp273. The carbonyl group at position 8 is observed near the backbone  $-NH$  group of Asp273. This may explain the increased activity of compounds with electronegative groups at this position and is consistent with the CoMFA red contour presented in this region. A large blue contour seen in the vicinity of position 9 suggests a favorable electropositive region, as corroborated by the presence of several amino acid carbonyl groups of Phe274, Asp273 and Gln184 in this region.

**Fig. 10** Docked conformation derived for compound **81** with the binding site of Aurora-A kinase. H-bonds are shown as *dotted black lines*. Active site amino acid residues and the inhibitor are represented as *stick model*. W2002 and W2004 represent water molecules, respectively



### Group-III

The default values of protomol bloat and threshold were applied and compound **81** is described in Fig. 10. A total of five H-bonds and one water-mediated interaction are formed between compound **81** and Aurora-A kinase. The pyrazole ring nitrogen at positions 5 and 6 forms H-bonds with the backbone of Ala213 ( $-N\cdots HN$ , 2.23 Å, 152.3°) and Glu211 ( $-NH\cdots O$ , 1.88 Å, 157.7°), respectively. The N atom at position 4 enters into a H-bonding interaction with the carbonyl group of Ala213 ( $-NH\cdots O$ , 2.38 Å, 117.8°). The carbonyl oxygen atom at position 9 and nitrogen atom at position 10 form H-bonds with the side chain of Lys162 ( $-O\cdots HN$ , 3.00 Å, 131.1° and  $-NH\cdots N$ , 3.35 Å, 143.9°), respectively. Interaction between the morpholine ring N at position 2 and the side chain guanidino group of Arg220 is mediated by a water bridge formed by water 2002 and water 2004 (2W1E.pdb, Fig. 10). The presence of residue Leu210 near position 7 of the pyrazole ring indicates that a bulky substituent is not favored in this region, which is in agreement with the 3D contour plots showing that a large sterically unfavorable yellow contour is located at this

position. Those binders with larger substituents at position 10 are generally better because the space in the receptor binding site is relatively large. The red contour near position 3 suggests a negative charge favorable region, as verified by the  $-NH_2$  of the guanidino group of Arg137 located herein. The presence of the  $-NH$  group on the backbone of Gly140 near position 11 indicates the preference of electronegative groups at this position, which can also be inferred from the CoMSIA red contour map. The blue contour observed near position 10 shows the region favorable for electropositive groups, which corresponds to interaction with the  $-NH$  group of Lys162.

#### Group-IV

The protomol bloat and threshold values were 0 and 0.43, respectively. Figure 11 depicts the interacting model of compound **119** with the kinase. Four H-bonds anchor the ligand into the binding site of Aurora-A. The thiazole ring nitrogen at position 2 acts as an acceptor to form an H-bond with the backbone  $-NH$  of Ala213 ( $-N\cdots HN$ , 2.00 Å, 162.6°). The N atom at position 3 forms another H-bond with the backbone of Ala213 ( $-NH\cdots O$ , 1.87 Å, 142.1°). The carbonyl oxygen and  $-OH$  atoms of the carboxyl group at the para-position of the phenyl ring form H-bonds with the guanidino group of Arg137 ( $-O\cdots HN$ , 1.97 Å, 154.9°) and the backbone O of Leu139 ( $-OH\cdots O$ , 2.47 Å, 62.5°), respectively. The substituent at position 1 can bind to a relatively shallow hydrophobic pocket formed by Val147, Ala160, Lys162 and Leu210 residues, which is in agreement with the CoMSIA small green contour present at this position. The yellow contour observed near position 6 indicates a sterically unfavorable region at this position. This is confirmed by docking results showing that bulkier groups at position 6 can lead to a steric clash with the side

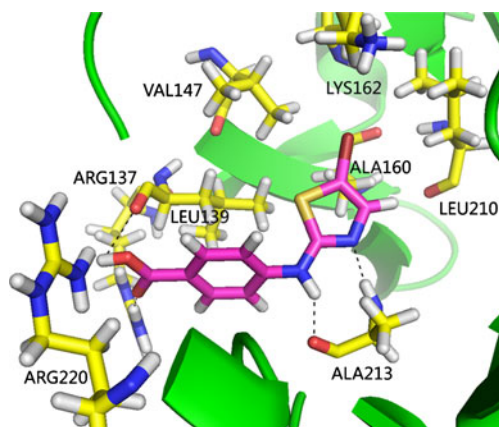


**Fig. 11** Docked conformation derived for compound **119** with the binding site of Aurora-A kinase. H-bonds are shown as *dotted black lines*. Active site amino acid residues and the inhibitor are represented as *stick model*

chain of residue Arg137. The presence of a blue contour near position 5 suggests the requirement of electropositive groups at this site and expects to have a favorable interaction with electronegative groups like the carbonyl backbone of Leu139. The magenta contour seen at position 4 indicates an H-bond acceptor favored region as verified by the H-bond donor group of  $-NH_2$  of Arg220 presented herein. The carbonyl group of Leu139 located at position 5 suggests the importance of H-bond donor groups at this position, which is also supported by the presence of an H-bond donor favorable red contour (CoMSIA model).

#### Group-V

The protomol bloat and threshold values were 0 and 0.43, respectively, and compound **176** is depicted in Fig. 12. There are four H-bonds and one water-mediated interaction between the inhibitor and binding site residues. The carbonyl oxygen at position 1 forms an H-bond with the backbone of Lys141 ( $-O\cdots HN$ , 2.01 Å, 162.6°). The pyrazole ring  $-N-$  and  $-NH$  atoms at positions 5 and 6 form H-bonds with the backbone atoms of Ala213 ( $-N\cdots HN$ , 2.16 Å, 155.9° and  $-NH\cdots O$ , 1.60 Å, 144.4°), respectively. The O atom at position 8 is located within H-bonding distance (3.45 Å) of the backbone of Thr217. Interaction between the nitrogen atom at position 2 and the side chain hydroxyl group of Thr217 is glued by a structural water molecule (w25, 3FDN.pdb). Docking results show that space around the substituent at position 1 is relatively large, and that this moiety seems to be exposed to the solvent, which is in line with the sterically favorable green contour presented herein. A large yellow contour at position 3 suggests a preference for small groups at this position, which is also validated by the docked

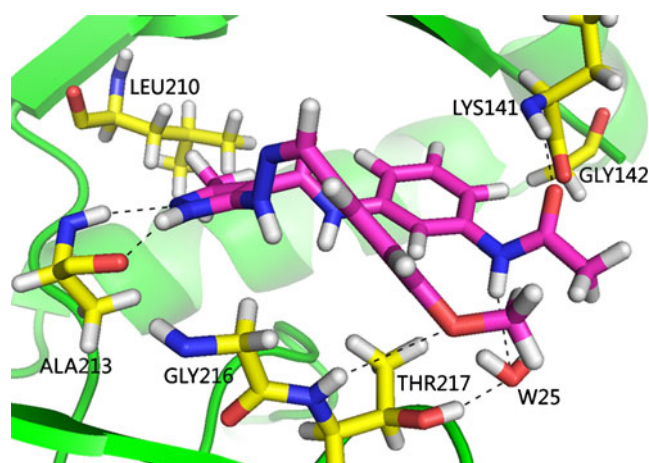


**Fig. 12** Docked conformation derived for compound **176** with the binding site of Aurora-A kinase. H-bonds are shown as *dotted black lines*. Active site amino acid residues and the inhibitor are represented as *stick model*. W25 represents water molecule

structure showing that substitution with bulky groups will have an unfavorable steric clash with the backbone atoms of Lys141 and Gly142. The electronegative favorable red contour near position 1 corresponds to the –NH– backbone of Lys141, which explains the increased activity of compounds with electronegative groups in this region. A small cyan contour near position 4 suggests H-bond donor groups are favored at this position as confirmed by the –NH group of Thr217 located nearby. The purple contour observed near position 7 indicates an H-bond acceptor favorable region, which is further supported by the presence of a backbone –NH group of Gly216 in this location.

#### Group-VI

The protomol bloat and threshold were set to 1 and 0.43, respectively, and compound **220** is displayed in Fig. 13. A total of three H-bonds and two water-mediated interactions exist between the ligand and the active site of Aurora-A kinase. The F atom at position 1 forms a H-bond with the side chain –NH of Lys162 (–F⋯HN, 2.35 Å, 136.1°). The pyrimidine ring nitrogen atoms at positions 2 and 3 form H-bonds with the side chain of Lys143 (–N⋯HN, 2.49 Å, 117.0° and –N⋯HN, 2.47 Å, 102.3°), respectively. The carbonyl oxygen at position 4 and the backbone –NH of Thr217 is linked by a water-mediated H-bond bridge (w455, 2NP8.pdb). Another water-mediated interaction is formed between the F atom at position 1 and the backbone carbonyl group of Ala273 through the water molecule w489. The side chain of Lys162 and Asp274 located near position 1 indicates that analogues with bulky substituents at the 1 position of the pyrimidine ring would have an unfavorable steric interaction. This is in accordance with

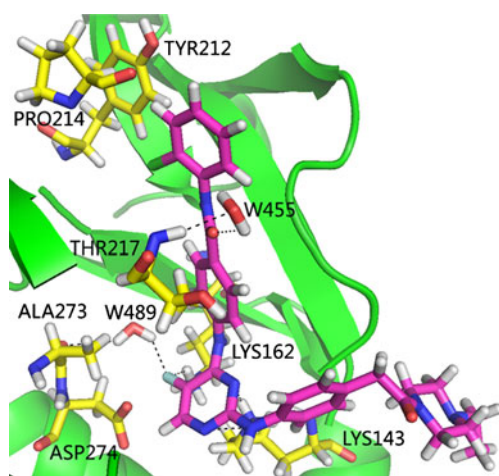


**Fig. 13** Docked conformation derived for compound **220** with the binding site of Aurora-A kinase. H-bonds are shown as *dotted black lines*. Active site amino acid residues and the inhibitor are represented as stick model. W455 and W489 represent water molecules, respectively

the 3D contour maps showing that a CoMSIA sterically unfavorable yellow polyhedron is observed at this position. The green contour seen near position 6 suggests a sterically favorable region, as corroborated by the docking structure showing that this space is relatively large, and extends even outside to the solvent. The red contours near positions 1 and 4 indicate that compounds with electronegative groups at these positions may have a favorable interaction with surrounding residues as shown by the side chain –NH of Lys162 and backbone –NH of Thr217 present nearby. The side chain hydroxyl group of Tyr212 and the backbone carbonyl group of Pro214 near position 8 suggests that hydrophilic groups are favored in this region, which is in line with the presence of a CoMSIA hydrophilic favorable white contour. A small white contour along with a small green contour is observed near position 9, suggesting that hydrophilic and bulky substituents are both favorable at this position, as demonstrated by the docking model showing that this moiety is located in the lower lobe of the solvent-exposed binding area.

In order to explore the similarities and differences in binding modes, the six docked complexes were superimposed together using PYMOL software ([www.pymol.org](http://www.pymol.org)). The common big ligand binding pocket was found to be constructed by 34 residues: Arg137, Pro138, Leu139, Gly140, Lys141, Gly142, Lys143, Val147, Ala160, Lys162, Leu164, Leu178, Glu181, Val182, Gln185, Leu194, Leu196, Leu208, Leu210, Glu211, Tyr212, Ala213, Pro214, Leu215, Gly216, Thr217, Tyr219, Arg220, Glu260, Asn261, Leu263, Ala273, Asp274 and Phe275 (residue numbering according to 3E5A.pdb).

Residues Arg137, Lys141, Lys143, Lys162, Glu181, Gln185, Glu211, Ala213, Thr217, Arg220, Ala273, Asp274 and Phe275 produced mainly H-bonds with the ligand, and amino acids Arg137, Lys141, Gly142, Val147, Ala160, Lys162, Leu178, Val182, Leu210, Thr217, Arg220 and Asp274 formed steric interactions or hydrophobic interactions (Val147, Ala160, Lys162, Leu210, Glu211, Tyr212, Ala213, Pro214 and Arg220) with inhibitors. Interestingly, Phe144 belongs only to G-I (3E5A.pdb) and cannot be found in other binding models, indicating that this residue might be more specific for G-I derivatives. It was also found that residue Ala213 (Ala212 in 2C6E) formed important H-bonding interactions in the five models G-I to G-V, but not in G-VI, suggesting that this residue plays a critical role in the recognition of Aurora-A by inhibitors.

We conclude that the results obtained from molecular docking and those from 3D-QSAR modeling can complement and validate each other, suggesting that the 3D-QSAR models generated in the present study are reasonable and could be utilized to derive useful information in the design of novel Aurora-A inhibitors.

## Conclusions

3D-QSAR studies using CoMFA and CoMSIA techniques were performed on six different chemical series of Aurora-A inhibitors. These studies yielded stable and statistically significant predictive models indicated by good performance with both internal and external validations. The 3D contour maps obtained from the optimal QSAR models in each group correlated well with the structural and functional features of the active binding sites identified from docking studies. One common residue, i.e., Ala213 (Ala212 in G-II), was found in the kinase active site that played a significant role in recognition of the inhibitors by presenting H-bonding interactions in five groups (not in G-VI). Other notable findings are listed in detail for each individual group as follows:

### Group-I

Hydrophobic interaction was found to govern the inhibitory activity of group I compounds by making the highest contribution of 46.4% in the optimal CoMSIA model. At position 4, a linker consisting of hetero atoms such as O and S between quinazoline and aromatic ring can enhance kinase activity. In addition, electronegative and hydrophilic substituents at position 8 can also improve the Aurora-A inhibitory activity of a compound.

### Group-II

Electrostatic interaction is more important in G-II molecules, showing a higher contribution of 54.6% in the best CoMFA model. A bulky substituent at position 6, and small and electronegative substituents at positions 8 and 10 would improve biological activity.

### Group-III

Electrostatic field contributes more than steric field (56.9% and 43.1%, respectively) in the best CoMSIA model, suggesting electrostatic interactions are more critical to G-III compounds. Substitution with small and electropositive groups at position 7, and relatively large and electropositive groups at position 10 might increase compound activity.

### Group-IV

The H-bond acceptor field exhibits a prominent contribution of 52.9% in the optimal CoMSIA model, which indicates the importance of H-bonding interactions to this kind of molecule. Bulky and H-bond donor substituents at position 5, and H-bond acceptor group at positions 4 and 6 would have a positive effect on bioactivity.

### Group-V

Electrostatic interactions were found to have a determinant effect on inhibitory potency by making a contribution of 58.6% in the best CoMSIA model. Bulky, electronegative and H-bond acceptor substituents at position 1, and electropositive and H-bond donor substituents at position 4 are favorable for biological activity.

### Group-VI

The hybrid effect of electrostatic and hydrophobic interactions is more crucial to the inhibitory activity of G-VI compounds. Substitution with small and electronegative groups at position 1, and bulky and hydrophilic groups at positions 8 and 9 may lead to an increase in compound activity.

To the best of our knowledge, this is the first study aimed at deriving predictive 3D-QSAR models for A-type Aurora kinase inhibitors. Moreover, the docking studies provided good insights into inhibitor–protein interactions at the molecular level. The good correlation between experimental and predicted  $pK_i$  or  $pIC_{50}$  values for test set compounds further indicated the robustness of the 3D-QSAR models. Thus, the derived models can be utilized in predicting the affinity of related analogues, guiding future structural modifications and synthesizing novel potent Aurora-A inhibitors.

**Acknowledgments** This work is supported financially by the National Natural Science Foundation of China (Grant No. 10801025) and the Fund of Northwest A&F University. We thank Dr. Ming Hao for helping with PCA analysis.

## References

1. Fu J, Bian M, Jiang Q, Zhang C (2007) *Mol Cancer Res* 5:1–10
2. Keen N, Taylor S (2004) *Nat Rev Cancer* 4:927–936
3. Andrews PD (2005) *Oncogene* 24:5005–5015
4. Jackson JR, Patrick DR, Dar MM, Huang PS (2007) *Nat Rev Cancer* 7:107–117
5. Giet R, Petretti C, Prigent C (2005) *Trends Cell Biol* 15:241–250
6. Glover DM, Leibowitz MH, McLean DA, Parry H (1995) *Cell* 81:95–105
7. Bischoff JR, Anderson L, Zhu Y, Mossie K, Ng L, Souza B, Schryver B, Flanagan P, Clairvoyant F, Ginther C, Chan CSM, Novotny M, Salomon DJ, Plowman GD (1998) *EMBO J* 17:3052–3065
8. Pollard JR, Mortimore M (2009) *J Med Chem* 52:2629–2651
9. Andersen CB, Wan Y, Chang JW, Riggs B, Lee C, Liu Y, Sessa F, Villa F, Kwiatkowski N, Suzuki M, Nallan L, Heald R, Musacchio A, Gray NS (2008) *ACS Chem Biol* 3:180–192
10. Zhou H, Kuang J, Zhong L, Kuo WL, Gray JW, Sahin A, Brinkley BR, Sen S (1998) *Nat Genet* 20:189–193
11. Dutertre S, Descamps S, Prigent C (2002) *Oncogene* 21:6175–6183

12. Barr AR, Gergely F (2007) *J Cell Sci* 120:2987–2996
13. Giet R, Uzbekov R, Cubizolles F, Le Guellec K, Prigent C (1999) *J Biol Chem* 274:15005–15013
14. Bolanos-Garcia VM (2005) *Int J Biochem Cell Biol* 37:1572–1577
15. Liu Q, Kaneko S, Yang L, Feldman RI, Nicosia SV, Chen J, Cheng JQ (2004) *J Biol Chem* 279:52175–52182
16. Nishida N, Nagasaka T, Kashiwagi K, Boland CR, Goel A (2007) *Cancer Biol Ther* 6:525–533
17. Gritsko TM, Coppola D, Paciga JE, Yang L, Sun M, Shelley SA, Fiorica JV, Nicosia SV, Cheng JQ (2003) *Clin Cancer Res* 9:1420–1426
18. Li DH, Zhu JJ, Firozi PF, Abbruzzese JL, Evans DB, Cleary K, Friess H, Sen S (2003) *Clin Cancer Res* 9:991–997
19. Reiter R, Gais P, Jutting U, Steuer-Vogt MK, Pickhard A, Bink K, Rauser S, Lassmann S, Höfler H, Werner M, Walch A (2006) *Clin Cancer Res* 12:5136–5141
20. Wang X, Zhou YX, Qiao W, Tominaga Y, Ouchi M, Ouchi T, Deng CX (2006) *Oncogene* 25:7148–7158
21. Ditchfield C, Johnson VL, Tighe A, Ellston R, Haworth C, Johnson T, Mortlock A, Keen N, Taylor SS (2003) *J Cell Biol* 161:267–280
22. Harrington EA, Bebbington D, Moore J, Rasmussen RK, Ajose-Adeogun AO, Nakayama T, Graham JA, Demur C, Hercend T, Diu-Hercend A, Su M, Golec JMC, Miller KM (2004) *Nat Med* 10:262–267
23. Hauf S, Cole RW, LaTerra S, Zimmer C, Schnapp G, Walter R, Heckel A, van Meel J, Rieder CL, Peters JM (2003) *J Cell Biol* 161:281–294
24. Mortlock AA, Foote KM, Heron NM, Jung FH, Pasquet G, Lohmann JJ, Warin N, Renaud F, Savi CD, Roberts NJ, Johnson T, Dousson CB, Hill GB, Perkins D, Hatter G, Wilkinson RW, Wedge SR, Heaton SP, Odedra R, Keen NJ, Crafter C, Brown E, Thompson K, Brightwell S, Khatri L, Brady MC, Kearney S, McKillop D, Rhead S, Parry T, Green S (2007) *J Med Chem* 50:2213–2224
25. Manfredi MG, Ecsedy JA, Meetze KA, Balani SK, Burenkova O, Chen W, Galvin KM, Hoar KM, Huck JJ, Leroy PJ, Ray ET, Sells TB, Stringer B, Stroud SG, Vos TJ, Weatherhead GS, Wysong DR, Zhang M, Bolen JB, Claiborne CF (2007) *Proc Natl Acad Sci USA* 104:4106–4111
26. Shimomura T, Hasako S, Nakatsuru Y, Mita T, Ichikawa K, Kodera T, Sakai T, Nambu T, Miyamoto M, Takahashi I, Miki S, Kawanishi N, Ohkubo M, Kotani H, Iwasawa Y (2010) *Mol Cancer Ther* 9:157–166
27. Bebbington D, Binch H, Charrier JD, Everitt S, Fraysse D, Golec J, Kay D, Knegtel R, Mak C, Mazzei F, Miller A, Mortimore M, O'Donnell M, Patel S, Pierard F, Pinder J, Pollard J, Ramaya S, Robinson D, Rutherford A, Studley J, Westcott J (2009) *Bioorg Med Chem Lett* 19:3586–3592
28. Coumar MS, Leou JS, Shukla P, Wu JS, Dixit AK, Lin WH, Chang CY, Lien TW, Tan UK, Chen CH, Hsu JT, Chao YS, Wu SY, Hsieh HP (2009) *J Med Chem* 52:1050–1062
29. Anderson K, Yang J, Koretke K, Nurse K, Calamari A, Kirkpatrick RB, Patrick D, Silva D, Tummino PJ, Copeland RA, Lai Z (2007) *Biochemistry* 46:10287–10295
30. Cramer RD III, Patterson DE, Bunce JD (1988) *J Am Chem Soc* 110:5959–5967
31. Klebe G, Abraham U, Mietzner T (1994) *J Med Chem* 37:4130–4146
32. Wang YH, Li Y, Yang SL, Yang L (2005) *J Comput Aided Mol Des* 19:137–147
33. Li Y, Wang YH, Yang L, Zhang SW, Liu CH (2006) *Internet Electron J Mol Des* 5:1–12
34. Xu X, Yang W, Li Y, Wang YH (2010) *Expert Opin Drug Discov* 5:21–31
35. Li Y, Wang YH, Yang L, Zhang SW, Liu CH, Yang SL (2005) *J Mol Struct* 733:111–118
36. Ai CZ, Wang YH, Li Y, Li YH, Yang L (2008) *QSAR Comb Sci* 27:1183–1192
37. Aliagas-Martin I, Burdick D, Corson L, Dotson J, Drummond J, Fields C, Huang OW, Hunsaker T, Kleinheinz T, Krueger E, Liang J, Moffat J, Phillips G, Pulk R, Rawson TE, Ultsch M, Walker L, Wiesmann C, Zhang B, Zhu BY, Cochran AG (2009) *J Med Chem* 52:3300–3307
38. Howard S, Berdini V, Boulstridge JA, Carr MG, Cross DM, Curry J, Devine LA, Early TR, Fazal L, Gill AL, Heathcote M, Maman S, Matthews JE, McMenamin RL, Navarro EF, O'Brien MA, O'Reilly M, Rees DC, Reule M, Tisi D, Williams G, Vinkovi M, Wyatt PG (2009) *J Med Chem* 52:379–388
39. Rawson TE, Rütth M, Blackwood E, Burdick D, Corson L, Dotson J, Drummond J, Fields C, Georges GJ, Goller B, Halladay J, Hunsaker T, Kleinheinz T, Krell HW, Li J, Liang J, Limberg A, McNutt A, Moffat J, Phillips G, Ran Y, Safina B, Ultsch M, Walker L, Wiesmann C, Zhang B, Zhou A, Zhu BY, Ru"ger P, Cochran AG (2008) *J Med Chem* 51:4465–4475
40. Heron NM, Anderson M, Blowers DP, Breed J, Eden JM, Green S, Hill GB, Johnson T, Jung FH, McMiken HH, Mortlock AA, Pannifer AD, Pauptit RA, Pink J, Roberts NJ, Rowsell S (2006) *Bioorg Med Chem Lett* 16:1320–1323
41. Jung FH, Pasquet G, Lambert-van der Brempt C, Lohmann JJ, Warin N, Renaud F, Germain H, De Savi C, Roberts N, Johnson T, Dousson C, Hill GB, Mortlock AA, Heron N, Wilkinson RW, Wedge SR, Heaton SP, Odedra R, Keen NJ, Green S, Brown E, Thompson K, Brightwell S (2006) *J Med Chem* 49:955–970
42. Leonard JT, Roy K (2006) *QSAR Comb Sci* 25:235–251
43. Jain AN (2003) *J Med Chem* 46:499–511
44. Zhao B, Smallwood A, Yang J, Koretke K, Nurse K, Calamari A, Kirkpatrick RB, Lai Z (2008) *Protein Sci* 17:1791–1797
45. Tari LW, Hoffman ID, Bensen DC, Hunter MJ, Nix J, Nelson KJ, McRee DE, Swanson RV (2007) *Bioorg Med Chem Lett* 17:688–691
46. Cheetham GM, Knegtel RM, Coll JT, Renwick SB, Swenson L, Weber P, Lippke JA, Austen DA (2002) *J Biol Chem* 277:42419–42422
47. Roy PP, Roy K (2008) *QSAR Comb Sci* 27:302–313